SIAM J. SCI. COMPUT.
Vol. 30, No. 6, pp. 2799–2816

HYBRID SIMULATIONS OF REACTION-DIFFUSION SYSTEMS IN POROUS MEDIA*

A. M. TARTAKOVSKY†, D. M. TARTAKOVSKY‡, T. D. SCHEIBE†, AND P. MEAKIN§

Abstract. Hybrid or multiphysics algorithms provide an efficient computational tool for combining micro- and macroscale descriptions of physical phenomena. Their use becomes imperative when microscale descriptions are too computationally expensive to be conducted in the whole domain, while macroscale descriptions fail in a small portion of the computation domain. We present a hybrid algorithm to model a general class of reaction-diffusion processes in granular porous media, which includes mixing-induced mineral precipitation on, or dissolution of, the porous matrix. These processes cannot be accurately described using continuum (Darcy-scale) models. The pore-scale/Darcy-scale hybrid is constructed by coupling solutions of the reaction-diffusion equations (RDE) at the pore scale with continuum Darcy-level solutions of the averaged RDEs. The resulting hybrid formulation is solved numerically by employing a multiresolution meshless discretization based on the smoothed particle hydrodynamics method. This ensures seamless noniterative coupling of the two components of the hybrid model. Computational examples illustrate the accuracy and efficiency of the hybrid algorithm.

Key words. multiphysics, multiscale, multiresolution, reactive transport, subsurface

AMS subject classifications. 76S05, 62P12

DOI. 10.1137/070691097

1. Introduction. Many physical phenomena are amenable to mathematical descriptions on a multiplicity of scales that range from atomistic to continuum. While fine-scale descriptions (e.g., molecular dynamics) can, in principle, describe such phenomena with the highest degree of fidelity, they often require computational capabilities that are not currently available and they are typically replaced with coarse-scale descriptions (e.g., differential equations) that provide an acceptable degree of fidelity at a fraction of the computational cost. Hybrid (multiphysics) numerical algorithms are rapidly gaining acceptance as a method of choice when coarse-scale continuum models fail to accurately describe a physical phenomenon in a small part of a computational domain. In the region or regions in which the continuum methods fail, they are replaced with their finer-scale counterparts (see, for example, the May/June 2005

*Received by the editors May 9, 2007; accepted for publication (in revised form) April 15, 2008; published electronically October 13, 2008. This research was supported by the Office of Science of the U.S. Department of Energy under Scientific Discovery through Advanced Computing. Partial support of this research was provided by project PL-MDT-PD05 funded by the Department of Energy National Nuclear Security Administration at the Pacific Northwest National Laboratory. PNNL is operated for the U.S. Department of Energy by Battelle under contract DE-AC06-76RL01830, and the Idaho National Laboratory is operated for the U.S. Department of Energy by the Battelle Energy Alliance under contract DE-AC07-05ID14517. This work was performed by an employee of the U.S. Government or under U.S. Government contract. The U.S. Government retains a nonexclusive, royalty-free license to publish or reproduce the published form of this contribution, or allow others to do so, for U.S. Government purposes. Copyright is owned by SIAM to the extent not limited by these rights.

http://www.siam.org/journals/sisc/30-6/69109.html

†Pacific Northwest National Laboratory, P.O. Box 999, Richland, WA 99352 (alexandre.tartakovsky@pnl.gov, tim.scheibe@pnl.gov).

‡Department of Mechanical and Aerospace Engineering, University of California, San Diego, La Jolla, CA 92093 (dmt@ucsd.edu).

§Idaho National Laboratory, P.O. Box 1625, MS 2025, Idaho Falls, Idaho ID 83415-2025 (paul.meakin@inl.gov).

issue of *Computing in Science and Engineering*).

The coupling of two (or more) mathematical models operating on vastly different spatial and/or temporal scales remains a major theoretical and computational challenge. Apart from fundamental issues, such as the propagation of noise between the discrete and continuum scales [2, 3, 4], a key to the success of a hybrid method is a computationally efficient implementation of the continuity and/or jump conditions on the interface(s) between different models (e.g., [17, 1]).

While general challenges posed by hybrid methods are common to most hybrids, their practical implementation is highly problem-specific and depends in large part on the scales of mathematical descriptions making up a given hybrid. Some of the recently proposed hybrid algorithms for reaction-diffusion systems, which are the focus of the present study, couple microscale (molecular dynamics) and mesoscale (kinetic Monte Carlo simulations) models [14], microscale (molecular dynamics) and macroscale (reaction-diffusion differential equation) models [10], mesoscale (lattice Boltzmann) and macroscale (reaction-diffusion differential equation) models [13], etc.

The choice of a particular hybrid algorithm for any physical system, including reaction-diffusion systems, is determined by the question under consideration. The goal of the work presented here is to simulate mixing-induced mineral precipitation in porous media. Macroscopic or Darcy-scale descriptions of this process, which rely on a coupled system of averaged reaction-diffusion equations, fail to account for highly localized precipitation that occurs along fluid-solid interfaces at the pore scale [19]. At the same time, pore-scale solutions of systems of reaction-diffusion equations (RDEs) are computationally expensive and require detailed knowledge of the pore geometry at a level that is rarely available on the macroscopic scales of interest. This scenario calls for a hybrid method in which microscopic pore-scale simulations are used in a narrow reaction zone, while macroscopic Darcy-scale simulations are used in the rest of a computational domain.

The application of grid-based methods to solve systems of RDEs in a domain consisting of interconnected pores, whose geometry changes with time as a result of precipitation, is a formidable task. One alternative is to employ lattice Boltzmann (LB) simulations inside the reaction zone and RDEs elsewhere, which gives rise to an LB-RDE hybrid. This class of hybrids has received considerable attention in a variety of applications. For some LB models, Chapman–Enskog expansions can be used to establish the equivalence between the LB and RDE representations of reaction-diffusion systems [7, and references therein]. This, in turn, allows for analytical derivation of interfacial conditions along the boundaries separating the LB and RDE computational domains [1]. In general, the derivation of the Chapman–Enskog coupling conditions might become problematic and their numerical counterparts have to be obtained via an iterative procedure, e.g., the iterative constrained runs scheme [11]. Such coupling procedures significantly increase the computational cost of the LB–RDE hybrids [13].

We present a computational alternative to LB-RDE hybrids, which replaces the LB microscale component with a smoothed particle hydrodynamics (SPH) solution of the RDEs. SPH is also used to solve the averaged RDEs to model diffusion and reactions at the macro scale (Darcy scale). Since the resulting hybrid does not require an iterative procedure to establish the proper coupling between solutions of the RDEs on the micro and macro scales, it is computationally efficient. A formulation and numerical implementation of the micro-macro scales (pore-Darcy scales) hybrid for a multicomponent reaction-diffusion system are described in sections 2 and 3. Computational examples and a detailed analysis of the performance of the pore-Darcy scales hybrid are provided in section 4.

2. Hybrid formulation for reaction-diffusion systems in porous media. Consider a reaction-diffusion process in a volume Ω^T of a fully saturated porous medium. Diffusion and reactions take place inside the fluid-filled pores, $\Omega_p^T \subset \Omega^T$. Pore-scale descriptions of this process solve appropriate reaction-diffusion equations that are defined over Ω_p^T and are subject to boundary conditions on fluid-solid interfaces $\partial\Omega_p^T$. Darcy-scale models treat the porous medium as a continuum, i.e., the corresponding reaction-diffusion equations are defined at every point $\mathbf{x} \in \Omega^T$. In a hybrid formulation, pore-scale simulations are carried out in Ω_d, a (small) portion of the porous medium Ω^T, while the Darcy-scale model is solved in the remainder of the porous medium Ω_c ($\Omega^T = \Omega_c \cup \Omega_d$). Pore- and Darcy-scale models of this reaction-diffusion system are presented in sections 2.1 and 2.2. The coupling of two models, along the interface separating Ω_c and Ω_d, is presented in section 2.3.

While the hybrid algorithm developed in this study is applicable to a large class of multicomponent reaction-diffusion systems in porous media, we formulate it in terms of mixing-induced heterogeneous precipitation. Mixing-induced heterogeneous precipitation involves a homogeneous reaction between two mixing solutes A and B, which forms a reaction product C that grows heterogeneously from a supersaturated solution. For simplicity, we disregard both the reverse homogeneous reaction and homogeneous nucleation. (The latter approximation implies that the super-saturation index is not large enough to support precipitation in the liquid phase.) Furthermore, we assume that precipitation occurs only as overgrowth on solid surfaces.

2.1. Pore-scale description and its SPH formulation. The subdomain $\Omega_d = \Omega_p(t) \cup \Omega_s(t)$, where the pore-scale simulations are conducted, consists of the fluid-filled pore space $\Omega_p(t)$ and the solid matrix $\Omega_s(t)$, with $F(t) = \Omega_s(t) \cap \Omega_p(t)$ denoting the corresponding (multiconnected) fluid-solid interface. Precipitation/dissolution causes the pore geometry, i.e., $\Omega_p(t)$, $\Omega_s(t)$, and $F(t)$, to change with time t.

Let $C^A(\mathbf{x}, t)$, $C^B(\mathbf{x}, t)$, and $C^C(\mathbf{x}, t)$ denote the normalized concentrations in the solvent of solutes A and B and the reaction product C. The concentrations are defined as the mass dissolved in a unit volume of fluid; the concentrations C^A and C^B are normalized with the corresponding initial concentrations $C^{A,0}$ and $C^{B,0}$; and the concentration C^C is normalized with $C^{A,0} + C^{B,0}$. The precipitation process can be described by a system of coupled reaction-diffusion equations [8],

$$\frac{\partial C^I}{\partial t} = \nabla \cdot (D^I \nabla C^I) - k^{AB} C^A C^B, \qquad I = A, B, \qquad \mathbf{x} \in \Omega_p, \tag{2.1a}$$

$$\frac{\partial C^C}{\partial t} = \nabla \cdot (D^C \nabla C^C) + k^{AB} C^A C^B - k \int_F (C^C - C_{eq}) \delta(\mathbf{x} - \mathbf{x}_f) \mathrm{d}a, \qquad \mathbf{x} \in \Omega_p, \tag{2.1b}$$

where $D^I > 0$ ($I = A, B, C$) are the molecular diffusion coefficients of species I in the solvent, $k^{AB} > 0$ and $k > 0$ are the rate coefficients of the homogeneous and heterogeneous reactions, $\mathbf{x}_f$ is a point on the interface F, and $\mathrm{d}a$ is an infinitesimally small element of F. It is important to recognize that the formulation (2.1) reflects several physical assumptions. First, it neglects diffusion in the solid phase, which is many orders of magnitude slower than its counterpart in the liquid phase. Second, it disregards the reverse reaction $C(aqueous) \rightarrow A + B$. Third, (2.1b) implies that precipitation/dissolution of the soluble reaction product C is described by a first-order

kinetic-reaction model on the fluid-solid interface,

$$D^C \nabla C^C \cdot \mathbf{n} = k(C^C - C_{eq}), \tag{2.2}$$

where C_{eq} is the concentration of C in equilibrium with the solid matrix, and $\mathbf{n}$ is the unit vector in the direction normal to the interface pointing toward the fluid. The normal velocity v_n, with which the fluid-solid interface at a point $\mathbf{x}_s$ advances into the liquid, is given by

$$v_n(\mathbf{x}_s) = \theta D^C \nabla C^C \cdot \mathbf{n}, \qquad \theta = \frac{C^{A,0} + C^{B,0}}{\rho_s}, \tag{2.3}$$

where $\rho_s > 0$ is the density of the precipitated solid phase. Parameters D^I ($I = A, B, C$), k^{AB}, k, and ρ_s are measurable quantities that are assumed to be known.

2.1.1. SPH representation of pore-scale RDEs. RDEs (2.1)–(2.3) defined on a highly irregular, evolving domain $\Omega_p(t)$ present significant challenges to grid-based methods, which require either sophisticated front tracking techniques or indirect interphase tracking schemes. Instead, we solve (2.1)–(2.3) with SPH, a meshless discretization method that is briefly described in the appendix. The subdomain Ω_d is discretized with two sets of points (the SPH "particles"): $\Omega_p(t)$ is discretized with "fluid" particles and $\Omega_s(t)$ is discretized with "solid" particles. Then any continuous scalar or vector function $A(\mathbf{x})$ is discretized by

$$A(\mathbf{x}) = \sum_{b \in \Omega_d} A_b V_b W(|\mathbf{x} - \mathbf{x}_b|, h) + \mathcal{O}(h^2), \tag{2.4}$$

where $\mathbf{x_b}$ is the position of particle b, $A_b = A(\mathbf{x}_b)$, V_b is the volume associated with particle b, and the summation is over both fluid and solid particles. The SPH weighting function W is a smooth bell-shaped function with a compact support or range h, i.e., $W(|\mathbf{x}| > h, h) = 0$, such that $\int_{\Omega_d} W(\mathbf{x}', h) \mathrm{d}\mathbf{x}' = 1$ and $\lim_{h \to 0} W = \delta(|\mathbf{x}|)$, where δ is the Dirac delta function. Using the interpolation scheme (2.4), equations (2.1) can be discretized as (appendix)

$$\frac{\partial C_a^I}{\partial t} = 4 \sum_{b \in \Omega_p} V_b \frac{D_a^I D_b^I}{D_a^I + D_b^I} \frac{C_a^I - C_b^I}{x_{ab}^2} \mathbf{x}_{ab} \cdot \nabla_a x_{ab} \frac{\partial W(x_{ab}, h)}{\partial x_{ab}} - k^{AB} C_a^A C_a^B, \quad I = A, B, \tag{2.5a}$$

$$\frac{\partial C_a^C}{\partial t} = 4 \sum_{b \in \Omega_p} V_b \frac{D_a^C D_b^C}{D_a^C + D_b^C} \frac{C_a^C - C_b^C}{x_{ab}^2} \mathbf{x}_{ab} \cdot \nabla_a x_{ab} \frac{\partial W(x_{ab}, h)}{\partial x_{ab}} + k^{AB} C_a^A C_a^B$$
$$-k \sum_{b \in \Omega_s} \Delta_b (C_a^C - C_{eq}) \mathcal{W}_b^{-1} W(x_{ab}, h_r), \qquad \mathcal{W}_b = \sum_{j \in \Omega_p} V_j W(x_{jb}, h_r). \tag{2.5b}$$

Here $\mathbf{x}_{ab} = \mathbf{x}_a - \mathbf{x}_b$; $x_{ab} = |\mathbf{x}_{ab}|$; $\sum_{b \in \Omega_p}$ and $\sum_{b \in \Omega_s}$ indicate summation over fluid and solid particles, respectively; and Δ_b denotes the reactive surface area (length in two-dimensional simulation) associated with solid particle b. The second term on the right-hand side of (2.5b) represents the heterogeneous reaction term obtained by discretization of the integral term in (2.1b), where $W(x, h_r)$ was used to approximate the Dirac delta function. The supports h_r and h of W in the reactions and diffusion

terms, respectively, are not, in general, the same. Reasoning that could be used to select the problem-specific values for h_r and h is provided in section 3.2. The normalization factor $\mathcal{W}_b$ guarantees that the total change of concentration due to the heterogeneous reaction is equal to $k\int_F (C^C - C_{eq})\mathrm{d}a$.

The SPH particles representing solids are frozen in space. We neglect the movement of fluid particles due to mineral precipitation, so that the hydrostatic conditions assumed in this study render fluid particles immobile. (Otherwise, their dynamics can be described by an SPH discretization of the Navier–Stokes equations.)

To describe the evolution of the fluid-solid interfaces due to precipitation and dissolution, we introduce "ghost" particles whose initial mass is zero and whose initial locations coincide with those of fluid particles. (The use of ghost particles is conceptually similar to the approach used in [16] to model solidification processes.) The mass of the ghost particles, $\tilde{m}_a$, changes due to the heterogeneous precipitation reaction according to (2.5b) as

$$\frac{\mathrm{d}\tilde{m}_a}{\mathrm{d}t} = k(C^{A,0} + C^{B,0}) \sum_{b\in\Omega_s} V_b \mathcal{W}_b^{-1} \Delta_b (C_a^C - C_{eq}) W(x_{ab}, h_r). \tag{2.6}$$

Once $\tilde{m}_a$ reaches the prescribed solid particle mass, m_0, the ghost particle is converted into a solid particle and the corresponding fluid particle is removed. Dissolution is modeled in a similar fashion by tracking the mass of solid particles according to (2.6). When the mass of a solid particle reaches zero, the solid particle is reclassified as a new fluid particle.

2.2. Darcy-scale (continuum) description. On the Darcy scale, the porous medium is treated as a continuum, and equations (2.1) are replaced by a system of averaged coupled reaction-diffusion equations

$$\frac{\partial \phi C^I}{\partial t} = \nabla\cdot(\phi \mathcal{D}^I \nabla C^I) - \phi k_{eff}^{AB} C^A C^B, \qquad I = A, B, \qquad \mathbf{x}\in\Omega_c, \tag{2.7a}$$

$$\frac{\partial \phi C^C}{\partial t} = \nabla\cdot(\phi \mathcal{D}^C \nabla C^C) + \phi k_{eff}^{AB} C^A C^B - \phi k_{eff}(C^C - C_{eq}), \qquad \mathbf{x}\in\Omega_c, \tag{2.7b}$$

where $\mathcal{D}^I$ $(I = A, B, C)$ are the effective diffusion coefficients; ϕ is the porosity of the porous medium; and k_{eff}^{AB} and k_{eff} are the effective rate coefficients for the homogeneous and heterogeneous reactions, respectively. In principle, the parameters ϕ, $\mathcal{D}^I$, k_{eff}^{AB}, and k_{eff} are measurable quantities, which are assumed to be known as long as the internal structure and topology of a porous medium are not significantly affected by precipitation and/or dissolution.

When the effects of precipitation and/or dissolution cannot be ignored, it is common to resort to ad hoc constitutive relationships between the changing porosity $\phi = \phi(\mathbf{x}, t)$ and other macroscopic parameters. For example, the Kozeny–Carman equation $K = c_0\phi^3(1-\phi)^{-2}\mathcal{A}^{-2}$ relates the permeability of a porous medium K to its porosity ϕ and specific surface area $\mathcal{A}$, c_0 being Kozeny's constant, [5, p. 166]; and the effective diffusion coefficient $\mathcal{D}$ can be related to its counterpart in free water D by $\mathcal{D} = \tau D$, where $0 < \tau < 1$ is the tortuosity of the porous medium [5, p. 115]. The validity of these phenomenological relationships, and their numerous alternatives discussed in [5], is debatable even in the absence of porosity-changing chemical processes. The hybrid algorithm described below obviates the necessity of using any

constitutive relationships of this kind, since it relies on the Darcy-scale description (2.7) only for the portion of the porous medium where changes in the pore geometry are insignificant and the parameters ϕ, k_{eff}^{AB}, and k_{eff} remain constant.

2.2.1. SPH representation of averaged Darcy-scale RDEs. Since the Darcy scale description does not explicitly account for the solid and liquid phases, only one kind of particle is used to discretize the computational domain Ω_c. By analogy with (2.5), the SPH discretization of the Darcy-scale RDEs yields (appendix)

$$\frac{\partial \phi_a C_a^I}{\partial t} = 4 \sum_{b \in \Omega_c} V_b \frac{\phi_a \phi_b \mathcal{D}_a^I \mathcal{D}_b^I}{\phi_a \mathcal{D}_a^I + \phi_b \mathcal{D}_b^I} \frac{C_a^I - C_b^I}{x_{ab}^2} \mathbf{x}_{ab} \cdot \bigtriangledown_a x_{ab} \frac{\partial W(x_{ab}, h)}{\partial x_{ab}}$$

$$- \phi_a k_{eff}^{AB} C_a^A C_a^B, \qquad I = A, B \tag{2.8a}$$

and

$$\frac{\partial \phi_a C_a^C}{\partial t} = 4 \sum_{b \in \Omega_c} V_b \frac{\phi_a \phi_b \mathcal{D}_a^C \mathcal{D}_b^C}{\phi_a \mathcal{D}_a^C + \phi_b \mathcal{D}_b^C} \frac{C_a^C - C_b^C}{x_{ab}^2} \mathbf{x}_{ab} \cdot \bigtriangledown_a x_{ab} \frac{\partial W(x_{ab}, h)}{\partial x_{ab}}$$

$$+ \phi_a k_{eff}^{AB} C_a^A C_a^B - \phi_a k_{eff} (C_a^C - C_{eq}). \tag{2.8b}$$

Darcy-scale (continuum) descriptions of reaction-diffusion processes in porous media are based on the averaging of microscopic RDEs over a representative volume of the porous media. Darcy-scale descriptions break down when significant gradients of concentrations on the scale of the representative volume are present [19]. If this occurs in a small region Ω_d of the computational domain Ω^T, hybrid simulations, which combine pore-scale simulations in Ω_d with Darcy-scale simulations in Ω_c, become attractive. The efficiency of a typical hybrid algorithm increases as the ratio $||\Omega^T||/||\Omega_d||$ increases. Whether Ω_d develops and whether the ratio $||\Omega^T||/||\Omega_d||$ is large is determined by the physical process under consideration via the initial and boundary conditions for (2.7). In this study we are concerned with reaction-diffusion processes with localized reaction fronts, which are formed, for example, when a solution with concentrations $C^A = 1$ and $C^B = 0$ is brought rapidly into contact with a solution with concentrations $C^A = 0$ and $C^B = 1$ in the same solvent.

2.3. Hybrid formulation. A hybrid pore-scale/Darcy-scale algorithm is constructed by combining the SPH representation of the pore-scale RDEs (2.5)–(2.6) defined on the domain Ω_d with the SPH representation of the Darcy-scale RDEs (2.8) defined on the domain Ω_c. The two components of the hybrid are coupled by imposing the continuity of normal fluxes of each species along the interface $\Gamma = \Omega_c \cap \Omega_d$ separating the two models,

$$D^I \mathbf{n} \cdot \nabla C^I{}_{|\Gamma_d} = \phi \mathcal{D}^I \mathbf{n} \cdot \nabla C^I{}_{|\Gamma_c}, \qquad I = A, B, C, \tag{2.9}$$

where the subscripts d and c indicate the side (discrete (pore) or continuum (Darcy)) of the hybrid interface Γ on which the relevant quantities are evaluated, and $\mathbf{n}$ is the unit vector normal to Γ pointing outside of the pore-scale domain.

3. Numerical implementation of the hybrid algorithm. The coupling of the two components of the pore-scale/Darcy-scale hybrid algorithm, i.e., the enforcement of the continuity conditions (2.9), is facilitated by employing SPH to numerically discretize both components of the hybrid.

3.1. Coupling of the pore-scale and Darcy-scale simulations. An SPH discretization of both continuum and discrete components of the hybrid provides a seamless way to couple the pore-scale and Darcy-scale descriptions of reaction-diffusion processes in porous media. Effective coupling of the continuum and discrete parts of the SPH hybrid model is achieved by combining the two sets of equations, (2.5) and (2.8), into one set that is valid over the entire computational domain Ω^T

$$\frac{\partial \omega_a C_a^I}{\partial t} = 4 \sum_{b \in \Omega_c \cup \Omega_p} V_b \frac{\omega_a \omega_b d_a^I d_b^I}{\omega_a d_a^I + \omega_b d_b^I} \frac{C_a^I - C_b^I}{x_{ab}^2} \mathbf{x}_{ab} \cdot \bigtriangledown_a x_{ab} \frac{\partial W(x_{ab}, h)}{\partial x_{ab}}$$

$$- \omega_a r_a^{AB} C_a^A C_a^B, \qquad I = A, B, \tag{3.1a}$$

$$\frac{\partial \omega_a C_a^C}{\partial t} = 4 \sum_{b \in \Omega_c \cup \Omega_p} V_b \frac{\omega_a \omega_b d_a^C d_b^C}{\omega_a d_a^C + \omega_b d_b^C} \frac{C_a^C - C_b^C}{x_{ab}^2} \mathbf{x}_{ab} \cdot \bigtriangledown_a x_{ab} \frac{\partial W(x_{ab}, h)}{\partial x_{ab}} + \omega_a r_a^{AB} C_a^A C_a^B$$

$$- \omega_a k_a^c (C_a^C - C_{eq}) - \omega_a k_a^d \sum_{b \in \Omega_s} \Delta_b (C_a^C - C_{eq}) \mathcal{W}_b^{-1} W(x_{ab}, h_r). \tag{3.1b}$$

Here

$$d_a^I = \begin{cases} D^I, & a \in \Omega_p, \\ \mathcal{D}^I, & a \in \Omega_c, \end{cases} \quad r_a^{AB} = \begin{cases} k^{AB}, & a \in \Omega_p, \\ k_{eff}^{AB}, & a \in \Omega_c, \end{cases}$$

$$k_a^c = \begin{cases} 0, & a \in \Omega_p, \\ k_{eff}, & a \in \Omega_c, \end{cases} \quad k_a^d = \begin{cases} k, & a \in \Omega_p, \\ 0, & a \in \Omega_c, \end{cases} \quad \omega_a = \begin{cases} 1, & a \in \Omega_p, \\ \phi, & a \in \Omega_c. \end{cases} \tag{3.2}$$

Note that the last term in (3.1b) vanishes in the Darcy-scale domain, since the soil grains and mineral surfaces are not explicitly represented there.

The symmetric form of the interactions between "pore-scale" and "Darcy-scale" particles in (3.1)–(3.2) ensures the continuity of mass fluxes across the interface between the Darcy-scale and pore-scale domains (appendix) and implicitly imposes the boundary condition (2.9). Parameters in the hybrid model, defined by (3.2), characterize the continuum properties of the porous media and/or properties of the solutions. These parameters can be measured by the standard laboratory or field experiments and they are tabulated for many soils and chemical compounds. The hybrid model does not require any additional parameters beyond those used in the Darcy-scale or pore-scale models and, hence, parameterization of the hybrid model can be easily achieved.

3.2. Multiresolution implementation of the hybrid algorithm. To increase the computational efficiency of the pore-scale/Darcy-scale hybrid algorithm, the spatial resolution of numerical simulations (i.e., the spacing between particles) was decreased in the continuum domain relative to its counterpart in the discrete domain. Particles in both domains were placed on the nodes of square lattices. In the discrete domain Ω_d, particles were placed on square lattices with a size $\Delta x = 0.25$ (in model length units). In the continuum domain Ω_c, the spacing between particles was increased from $\Delta x = 0.25$ near the boundary Γ to $\Delta x = 1$ away from Γ. The support length for each particle was set at

$$h_i = 4 \Delta x_i, \tag{3.3}$$

where Δx_i is the size of the lattice cell on which particle i is located. This defines a smoothing length over which each particle interacts with approximately 50 neighbors. Finally, h_r was set to

$$h_r = \sqrt{2}\Delta x + 0.01\Delta x \tag{3.4}$$

so that only one layer of fluid particles can react with the solid particles and vice versa. Upon setting $h_{ij} = (h_i + h_j)/2$, this leads to the following multiresolution SPH formulation:

$$\frac{\partial \omega_a C_a^I}{\partial t} = 4 \sum_{b\in\Omega_c\cup\Omega_p} V_b \frac{\omega_a\omega_b d_a^I d_b^I}{\omega_a d_a^I + \omega_b d_b^I} \frac{C_a^I - C_b^I}{x_{ab}^2} \mathbf{x}_{ab}\cdot\bigtriangledown_a x_{ab} \frac{\partial W(x_{ab}, h_{ij})}{\partial x_{ab}}$$
$$- \omega_a r_a^{AB} C_a^A C_a^B, \qquad I = A, B, \tag{3.5a}$$

$$\frac{\partial \omega_a C_a^C}{\partial t} = 4 \sum_{b\in\Omega_c\cup\Omega_p} V_b \frac{\omega_a\omega_b d_a^C d_b^C}{\omega_a d_a^C + \omega_b d_b^C} \frac{C_a^C - C_b^C}{x_{ab}^2} \mathbf{x}_{ab}\cdot\bigtriangledown_a x_{ab} \frac{\partial W(x_{ab}, h_{ij})}{\partial x_{ab}} + \omega_a r_a^{AB} C_a^A C_a^B$$
$$- \omega_a k_a^c (C_a^C - C_{eq}) - \omega_a k_a^d \sum_{b\in\Omega_s} \Delta_b (C_a^C - C_{eq}) \mathcal{W}_b^{-1} W(x_{ab}, h_r). \tag{3.5b}$$

An extensive discussion of the multiresolution SPH method can be found in [12] and references therein.

3.3. Time integration. Integration of the SPH equations (3.5) can be carried out using various explicit [15] or fully implicit [6] schemes. To improve the algorithm's efficiency, an adaptive particle time stepping can be used [12].

In this study, we employed an explicit Euler time stepping integration method,

$$C_a^I(t + \Delta t) = C_a^I(t) + \Delta t \frac{\mathrm{d}C_a^I(t)}{\mathrm{d}t}, \tag{3.6}$$

where the time step Δt satisfies the following conditions:

$$\Delta t < \min\left(\epsilon_1 \frac{\Delta x_a^2}{d_a^I}, \frac{\epsilon_2}{k_a^{AB}}, \epsilon_3 \frac{\Delta x_a}{k}\right). \tag{3.7}$$

Our numerical experiments have shown that setting $\epsilon_1 = \epsilon_2 = \epsilon_3 = 0.25$ provides a stable and accurate solution. (See also [16], where the first of these inequalities, $\epsilon_1 = 0.25$, was postulated.)

4. Computational examples. To analyze the accuracy and robustness of the different components of the hybrid multiresolution SPH model, we used several reaction-diffusion systems for which analytical solutions are available. In section 4.1, we investigate the evolution of planar and circular precipitation fronts to validate the pore-scale part of the hybrid algorithm. In section 4.2, we use diffusion of a passive scalar in porous media as a testbed for analyzing the accuracy of the multiresolution algorithm relative to that of its single-resolution counterpart. In section 4.3, we employ the pore-scale/Darcy-scale hybrid algorithm to model mixing-induced precipitation in porous media. The accuracy of the pore-scale/Darcy-scale hybrid algorithm is verified by comparing results of hybrid simulations with results obtained from pore-scale simulations.

4.1. Dynamics of precipitation fronts. The evolution of a planar or circular precipitation front (i.e., a solid-fluid interface) $F(t)$ can be described on the pore scale by the diffusion-reaction equation

$$\frac{\partial u}{\partial t} = D\frac{\partial^2 u}{\partial x^2}. \tag{4.1}$$

The initial position of the planar front is $F(\mathbf{x}, 0) = F_0(\mathbf{x})$ and the initial concentration is $u(\mathrm{x}, 0) = u_0$. The conditions on the moving front $F(t)$ are

$$D\frac{\partial u}{\partial x} = k(u - u_{eq}), \tag{4.2a}$$

$$\frac{\mathrm{d}F}{\mathrm{d}t} = \frac{k}{\rho_s}(u - u_{eq}). \tag{4.2b}$$

The front is driven by the prescribed concentration $u(L, y, t) = u_0$ at the inlet $x = L$, and periodic boundary conditions are used in the y direction. For circular precipitation fronts, the Cartesian coordinate system (x, y) is replaced with a radial coordinate system, in which the boundary conditions take the form $u(r = L, t) = u_0$.

For slowly moving interfaces, the time derivative in (4.1) can be disregarded, which leads to an explicit analytical solution for the planar interface dynamics,

$$F(t) = \frac{D}{k} + L - \sqrt{\left(\frac{D}{k} + L - F_0\right)^2 - 2D\frac{u_0 - u_{eq}}{\rho_s}t}, \tag{4.3}$$

and an implicit analytical solution for the circular interface dynamics,

$$F(t) - F_0 - \frac{k}{2D}\left[F(t)^2 \ln\left(\frac{F(t)}{L}\right) - \frac{1}{2}F(t)^2 - F_0^2 \ln\left(\frac{F_0}{L}\right) + \frac{1}{2}F_0^2\right] = -\frac{ku_{eq}}{\rho_s}t. \tag{4.4}$$

Figure 1 provides a comparison between these analytical solutions and their numerical counterparts obtained using the two-dimensional SPH equations (2.5)–(2.6). The analytical and SPH solutions for the planar interface are nearly identical (Figure 1(a)). The slight disagreement between the analytical and SPH solutions for the circular interface at large times (Figure 1(b)) can be explained by the fact that, in the SPH model, particles are located on a square lattice which is not an ideal discretization for a radial growth process.

4.2. Diffusion of a passive scalar. Diffusion of a passive scalar in a porous medium fully saturated with a liquid provides an ideal setting for the analysis of various aspect of the proposed hybrid algorithm. We start by investigating the errors introduced by the coarsening inherent in the multiresolution implementation of the SPH algorithm. This is accomplished by comparing the numerical (fine-scale) single-resolution and multiresolution SPH solutions of a continuum diffusion model with each other and their analytical counterpart. Having established the accuracy of the SPH solver, we employ the SPH hybrid algorithm to analyze a multiscale diffusion that couples the pore and Darcy scales.

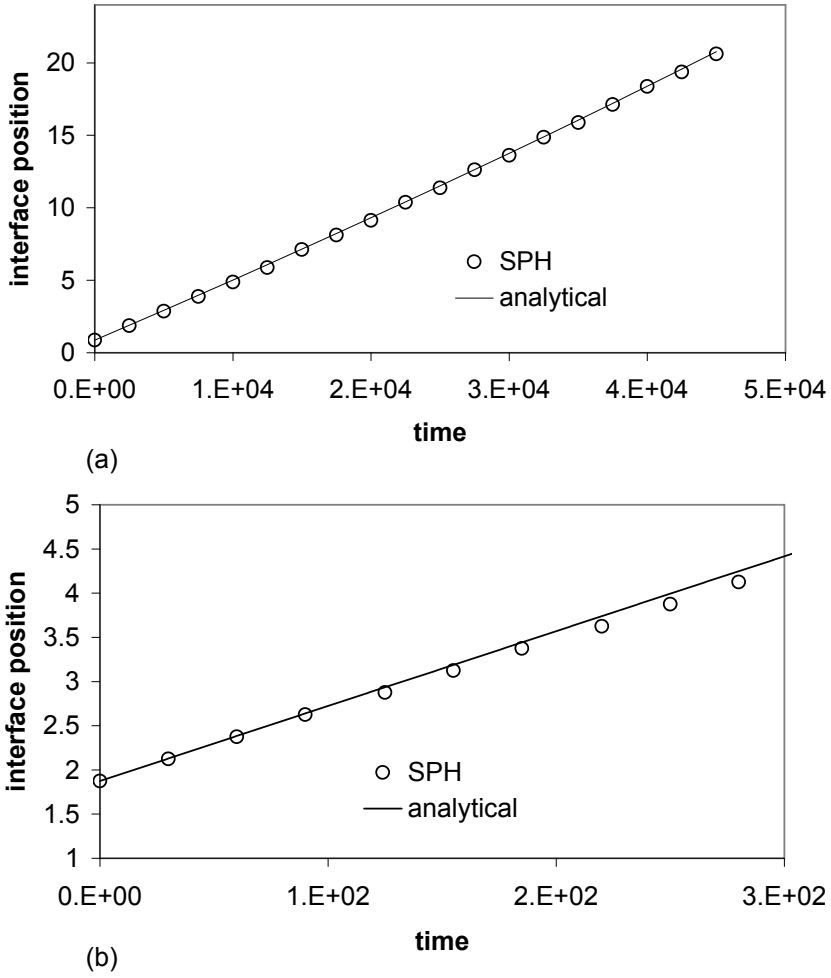

FIG. 1. *Positions of the planar* (a) *and circular* (b) *interfaces as functions of time, computed using the SPH simulations (circles) and analytically (solid lines).*

4.2.1. SPH simulations of diffusion on the Darcy (continuum) scale. Consider the two-dimensional diffusion equation $\partial u/\partial t = D\nabla^2 u$ on $\Omega^T = [0, L]\times[0, B]$ subject to the boundary and initial conditions

$$u(1, y, t) = 1, \quad \frac{\partial u}{\partial x}(L, y, t) = 0, \quad u(x, 0, t) = u(x, B, t), \quad u(x, y, 0) = 0. \tag{4.5}$$

The analytical solution of this problem,

$$u(x, t) = 1 - \frac{4}{\pi}\sum_{n=1}^{\infty}\frac{1}{n}\exp\left[-\frac{(1+2n)^2\pi^2}{4L^2}Dt\right]\sin\left[\frac{(1+2n)\pi x}{2L}\right], \tag{4.6}$$

was used to determine the relative accuracy of the single- and multiresolution implementations of the SPH solver. In fine-grained single-resolution simulations, the SPH particles were placed on a square lattice with a lattice size of $\Delta x = 0.25$ (in the model

units of length). In multiresolution simulations, the central part of the computational domain, $x \in [L/4, 3L/4]$, was discretized with small particles placed on a square lattice with $\Delta x = 0.25$, while the rest of the domain was discretized with large particles placed on a square lattice with $\Delta x = 1$. In both simulations $D = 0.5$, $L = 31$, and $B = 8$.

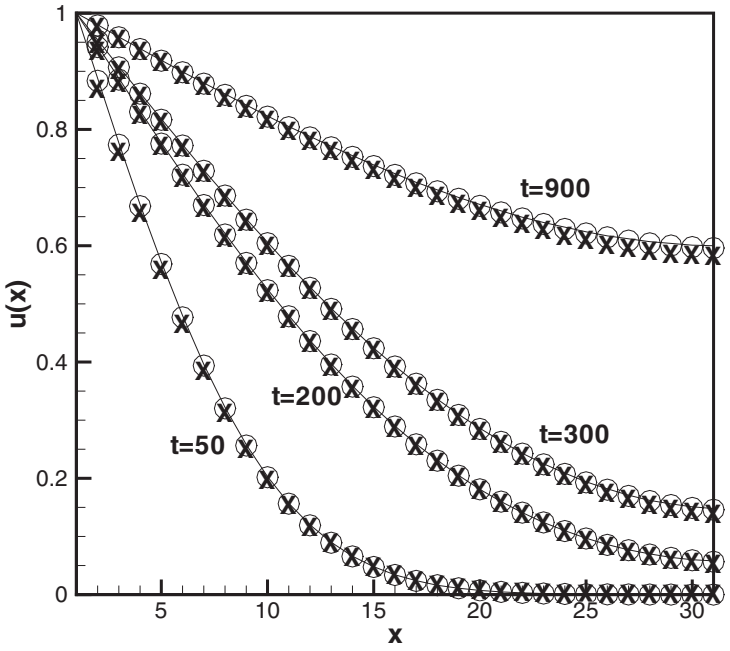

FIG. 2. *Solutions of the diffusion equation obtained analytically (solid line) and from the single resolution (circles) and multiresolution (X symbols) SPH simulations.*

Figure 2, which compares these numerical simulations with the analytical solution (4.6), demonstrates that both fine- and multiresolution SPH algorithms yield accurate solutions.

4.2.2. Hybrid simulations of diffusion on the pore and Darcy scales. Diffusion in a saturated porous medium composed of nonoverlapping circular grains (Figure 3) that is driven by the initial and boundary conditions (4.5) was used to illustrate the hybrid model. On the Darcy scale the evolution of the concentration field can be described by the analytical solution (4.6). On the pore scale, the process is described by the diffusion equation $\partial u/\partial t = D\nabla^2 u$ in Ω_p. The initial and boundary conditions (4.5) are supplemented with the boundary condition on the solid-liquid interfaces Γ_s,

$$\mathbf{n} \cdot \nabla u = 0, \qquad \mathbf{x} \in \Gamma_s. \tag{4.7}$$

First, SPH simulations were used to solve the diffusion problem on the pore scale throughout the whole computational domain. The single-resolution discretization of

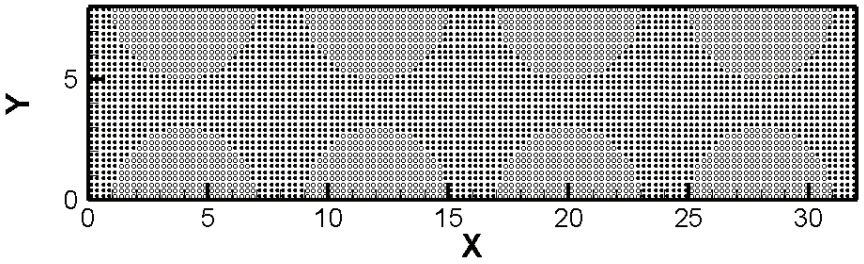

(a)

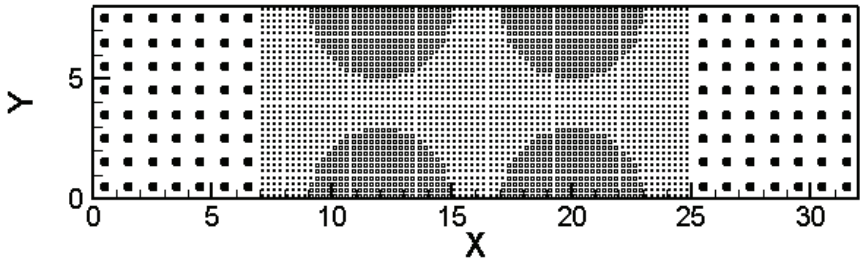

(b)

FIG. 3. *A schematic representation of the porous medium used in the pore-scale* (a) *and hybrid pore-scale/Darcy-scale* (b) *simulations. The open circles represent particles corresponding to the soil grains. The filled circles represent particles corresponding to the pore space filled with a fluid.*

the computational domain is shown in Figure 3(a), where the open circles represent the particles used to discretize the porous matrix and the filled circles designate the fluid particles inside the pores. Figure 4 shows the resulting averaged concentration,

$$\langle u(x,t)\rangle = \frac{1}{A(x)}\int_{y(x)} u(x,y',t)\mathrm{d}y', \tag{4.8}$$

where $A(x)$ is the cross-sectional area (length in two dimensions) of the pore space.

The pore-scale simulations shown in Figure 4 were carried out using a molecular diffusion coefficient of $D = 0.5$. By fitting the analytical solution for the continuum model (4.6) to the average concentration computed with the pore-scale SPH simulations we found that the corresponding effective diffusion coefficient is $\mathcal{D} = 0.31$.

Next, we employed the hybrid algorithm in which the pore-scale simulations in the central segment of the porous medium, $x \in [7, 27]$, are coupled with the Darcy-scale (continuum) simulations in the rest of the computational domain (Figure 3b). Diffusion is driven by the initial and boundary conditions (4.5). The pore- and Darcy-scale simulations are coupled through the continuity conditions (2.9). Figure 4 demonstrates the good agreement between the hybrid and pore-scale solutions of the diffusion equation, thus confirming the accuracy of the proposed hybrid algorithm.

4.3. Mixing-induced precipitation in porous media. As a final example, we consider mixing-induced precipitation in the porous medium depicted in Figure 3.

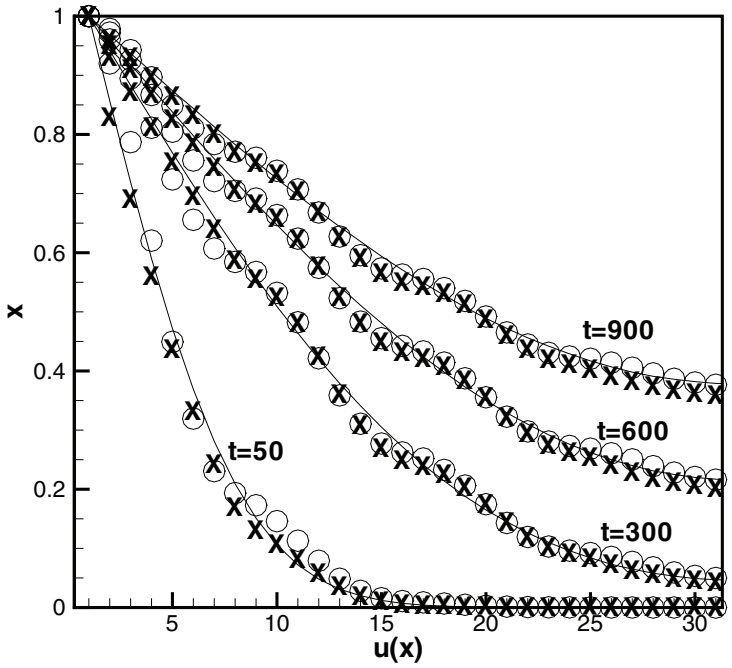

FIG. 4. *Temporal snapshots of the concentration profiles computed analytically (solid line) and numerically with both the fine, pore-scale SPH simulations (circles) and the hybrid, pore-scale/Darcy-scale simulations (X symbols).*

A hybrid simulation of this process was conducted and validated against a numerical solution obtained with the pore-scale model.

4.3.1. Pore-scale SPH simulations. First, pore-scale simulations were conducted over the whole computational domain, in which diffusion of solutes A and B and production and precipitation of the reaction product C are governed by equations (2.5) subject to the boundary conditions

$$C^A(0,y,t) = C^B(L,y,t) = 1, \quad \frac{\partial C^A}{\partial x}(L,y,t) = \frac{\partial C^B}{\partial x}(0,y,t) = 0,$$
$$\frac{\partial C^C}{\partial x}(0,y,t) = \frac{\partial C^C}{\partial x}(L,y,t) = 0 \tag{4.9}$$

and the initial conditions

$$C^A(x,y,0) = \begin{cases} 1, & x \le 16, \\ 0, & x > 16, \end{cases} \quad C^B(x,y,0) = \begin{cases} 0, & x \le 16, \\ 1, & x > 16, \end{cases} \quad C^C(x,y,0) = 0. \tag{4.10}$$

As before, the periodic boundary conditions were prescribed at $y = 0$ and $y = B$. The initial geometry of the pore matrix is shown in Figure 3(a), and its evolution as a result of precipitation is described by (2.3).

The left column in Figure 5 shows three temporal snapshots of the pore-scale SPH simulations of this reaction-diffusion system for $L = 31$, $B = 8$, $D = 0.5$,

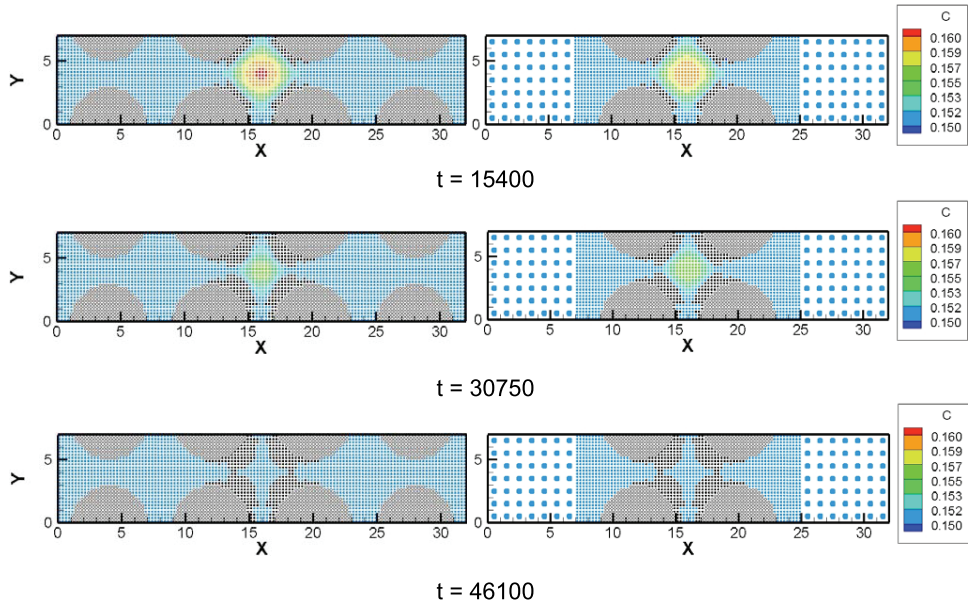

FIG. 5. *Snapshots of the distribution of precipitates (the filled circles) and the concentration of solute C (the color scale) at three different times. The open circles denote particles representing soil grains. The left and right columns depict results of the pore-scale and hybrid simulations, respectively.*

$k^{AB} = 1.5$, and $k = 20$. Precipitation of the reacting product C (the black particles in Figure 5) modifies the structure of the porous medium, thus leading to changes in its effective properties, including porosity, effective diffusion coefficient, and effective reaction rates. As should be expected, these processes occur only in the narrow reaction zone separating the solutions of the two reactants A and B.

4.3.2. Hybrid simulations. The presence of a small region within a computational domain in which a coarse-grain description breaks down is, of course, the raison d'être for a hybrid algorithm. Since evolution of the pore geometry cannot be accurately described on the Darcy (continuum) scale, we employed the hybrid pore-scale/Darcy-scale algorithm. It combines a pore-scale simulation in the central part of the computational domain with a continuum reaction-diffusion description elsewhere (Figure 3(b)).

To parameterize the Darcy-scale model, we obtained a steady-state finite-element solution of the one-dimensional version of (2.7) subject to the boundary conditions $C^A(0) = 1$, $C^A(L) = 0$, $C^B(0) = 0$, $C^B(L) = 1$, and $C^C(0) = C^C(L) = 0$. This solution was fitted to the y-averaged steady-state SPH solution of the corresponding pore-scale model with $L = 31$, $B = 8$, $D = 0.5$, $k^{AB} = 1.5$, and $k = 20$ to yield the effective transport parameters $\mathcal{D}^I = 0.31$ $(I = A, B, C)$, $k_{eff}^{AB} = 0.98$, and $k_{eff} = 3.3$.

The right column in Figure 5 presents the results of the hybrid pore-scale/Darcy-scale simulations. Figure 6 shows the temporal evolution of the porosity of the portion of the porous medium affected by precipitation, $x \in [8, 24]$, obtained with the pore-scale and hybrid simulations. It can be seen that the two are in close agreement.

In the examples presented here, the hybrid algorithm allowed the number of SPH particles to be reduced from 4096 in the pore-scale simulations over the whole computational domain to 2416 in the hybrid pore-scale/Darcy-scale simulations. In

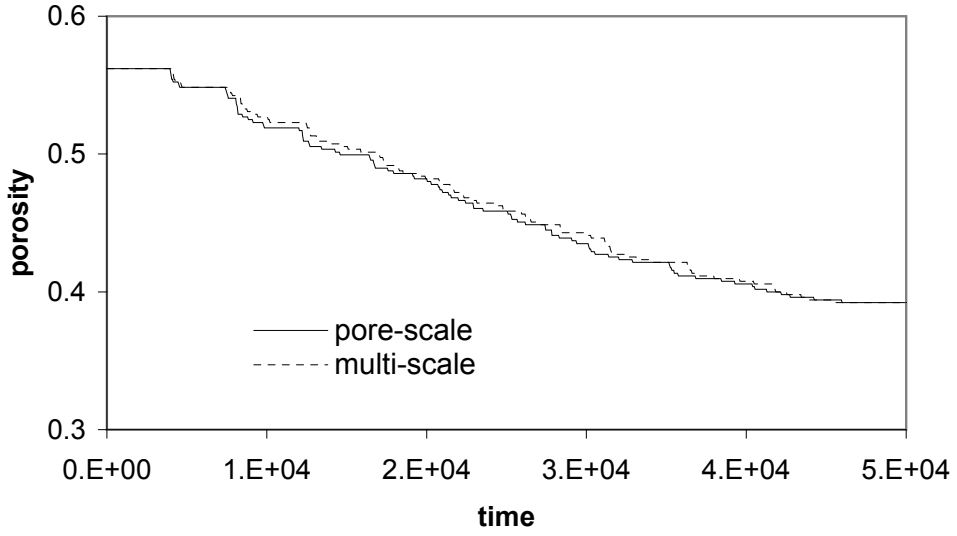

FIG. 6. *The change in porosity of the portion of a porous medium located between* $x = 8$ *and* $x = 24$ *computed with the pore-scale (the solid line) and hybrid pore-scale/Darcy-scale (the broken line) simulations.*

these simulations, the domain of the pore-scale simulations occupied half the total computational domain. In real applications of the hybrid model, this ratio is expected to be orders of magnitude smaller, so that the savings in the number of particles are expected to be substantially larger. The savings can be increased further by reducing the number of particles used to discretize the continuum (Darcy-scale) subdomains as the distance from the nearest pore-scale domain increases. Since the number of operations in SPH simulations increases linearly with the number of particles, the hybrid algorithm allows for a significant reduction in computational time.

5. Conclusions. The main goal of this study was to develop a computationally efficient hybrid algorithm for modeling reaction-diffusion processes in porous media on both the pore scale and the Darcy (continuum) scale. This goal was achieved by employing an SPH approach as the numerical engine of the hybrid model. Our study leads to the following major conclusions:

- The use of SPH for discretization of reaction-diffusion models on the pore and continuum scales allows for a seamless noniterative coupling of the two descriptions.
- Conducting SPH simulations at multiple resolutions can further enhance the efficiency of the hybrid algorithm. This was accomplished without compromising the accuracy of the hybrid model.
- Parameters in the hybrid model characterize the continuum properties of the porous media and/or properties of the solutions and solvent. They can be measured by the standard laboratory or field experiments, and are tabulated for many soils and chemical compounds. A parameterization of the hybrid model does not require any additional parameters beyond those used in the Darcy-scale or pore-scale models.
- The effective parameters ($\mathcal{D}_a^I$, k_{eff}^{AB} and k_{eff}) may change as a result of precipitation/dissolution. Since the functional dependence of these parameters on the amount of precipitates is not well understood, the reliability of stan-

dard, single-scale continuum models of reactive transport is hard to ascertain. In the proposed hybrid model, the continuum representation and effective parameters are only used in the part of computational domain where no significant precipitation occurs. As a result, the effective parameters do not change during simulations, which significantly increases the fidelity of the hybrid model's predictions.

The present study focused on diffusion as the main mechanisms of solute transport. In many applications, e.g., contaminant transport in subsurface environments, advection also plays an important role. We leave this problem for future research.

In the present study, the location of the pore-scale and Darcy-scale subdomains was dictated by the localized precipitate growth. The area where precipitations occurred could be easily deduced from boundary and initial conditions. Under more general conditions, easily implemented criteria must be developed (e.g., based on large concentrations and large concentration gradients) to determine the locations of subdomains in which pore-scale modeling might be required.

Appendix. SPH discretization. An SPH meshless conservative interpolation scheme for the diffusion equation

$$\frac{\partial u}{\partial t} = \nabla \cdot (D \nabla u), \qquad \mathbf{x} \in \Omega, \quad t > 0, \tag{A.1}$$

with [16]

$$\nabla \cdot (D \nabla u) \approx \int_{\Omega} [D(\mathbf{x}) + D(\mathbf{x}')][u(\mathbf{x}, t) - u(\mathbf{x}', t)] F(\mathbf{x} - \mathbf{x}', h) \mathrm{d}\mathbf{x}', \tag{A.2}$$

where F is defined by

$$\mathbf{x} F(\mathbf{x}, h) = \nabla_x W(\mathbf{x}, h). \tag{A.3}$$

By expanding the integrand in (A.2) in a Taylor series around $\mathbf{x}$, it can be shown that this term is a second-order approximation, $\mathcal{O}(h^2)$, of the Laplacian in (A.1).

Next, the computational domain is discretized with N "particles," i.e., (A.2) is approximated by

$$\frac{\mathrm{d}u_a}{\mathrm{d}t} = \sum_b V_b (D_a + D_b)(u_a - u_b) F(\mathbf{x}_a - \mathbf{x}_b, h), \qquad a = 1, \ldots, N, \tag{A.4}$$

where V_b is the volume (area in two spatial dimensions) of the portion of the computational domain Ω associated with particle b, and the summation is over all particles within distance h from particle a. Due to the compactness of the kernel W, other particles do not contribute to the change in the concentration of particle a. For highly varying diffusion coefficients $D(\mathbf{x})$, a better approximation of (A.1), which conserves the continuity of mass fluxes $-D\nabla u$ and has an accuracy comparable to that of finite-difference methods, can be achieved by replacing the coefficient $D_a + D_b$ in (A.4) with $4D_aD_b/(D_a + D_b)$ [9],

$$\frac{\mathrm{d}u_a}{\mathrm{d}t} = 4 \sum_b V_b \frac{D_a D_b}{D_a + D_b} (u_a - u_b) F(\mathbf{x}_a - \mathbf{x}_b, h), \qquad a = 1, \ldots, N. \tag{A.5}$$

This is the SPH representation used in our analysis.

We employed a quintic spline kernel [17 and references therein] for which $F \leq 0$, $F(-\mathbf{x}, h) = F(\mathbf{x}, h)$, and

$$W(\mathbf{x}_a - \mathbf{x}_b, h) = W(x_{ab}, h), \qquad x_{ab} = ||\mathbf{x}_a - \mathbf{x}_b||. \tag{A.6}$$

According to (A.3), this gives

$$F(x_{ab},h)=\frac{(\mathbf{x}_a-\mathbf{x}_b)\cdot\bigtriangledown_a x_{ab}}{x_{ab}^2}\frac{\partial W(x_{ab},h)}{\partial x_{ab}}. \tag{A.7}$$

In general, the volume V_a occupied by particle a can be found from

$$V_a^{-1}=\sum_b W(x_{ab},h),\qquad a=1,\dots,N. \tag{A.8}$$

In the two-dimensional SPH simulations reported in this study, particles were placed on a uniform square lattice so that the volume (area in two-dimensional simulations) occupied by each particle is

$$V_a=\Delta x^2,\qquad a=1,\dots,N, \tag{A.9}$$

where Δx is the size of the elements of the square lattice.

Finally, due to the antisymmetric form of the terms in the SPH discretization scheme, the summation over all N particles in a closed system yields

$$\sum_{a=1}^{N} V_a\frac{\mathrm{d}u_a}{\mathrm{d}t}=0. \tag{A.10}$$

In other words, the SPH discretization of the diffusion equation is explicitly mass conservative.

REFERENCES

[1] P. Albuquerque, D. Alemani, B. Chopard, and P. Leone, *A hybrid lattice Boltzmann finite difference scheme for the diffusion equation*, Internat. J. Mult. Comput. Engrg., 4 (2), 2006.

[2] F. J. Alexander, A. L. Garcia, and D. M. Tartakovsky, *Algorithm refinement for stochastic partial differential equations:* 1. *Linear diffusion*, J. Comput. Phys., 182 (2002), pp. 47–66.

[3] F. J. Alexander, A. L. Garcia, and D. M. Tartakovsky, *Algorithm refinement for stochastic partial differential equations:* Ii. *Correlated systems*, J. Comput. Phys., 207 (2005), pp. 769–787.

[4] F. J. Alexander, A. L. Garcia, and D. M. Tartakovsky, *Noise in algorithm refinement methods*, Comput. Sci. Engrg., 7 (2005), pp. 32–38.

[5] J. Bear, *Dynamics of Fluids in Porous Media*, Elsevier, New York, 1972.

[6] A. K. Chaniotis, C. E. Frouzakis, J. C. Lee, A. G. Tomboulidies, and D. A. B. Poulikakos, *Remeshed smoothed particle hydrodynamics for the simulation of laminar chemically reactive flows*, J. Comput. Phys., 191 (2003), pp. 1–17.

[7] S. Chen and G. D. Doolen, *Lattice Boltzmann method for fluid flows*, Ann. Rev. Fluid Mech., 30 (1998), pp. 329–364.

[8] B. Chopard, P. Luthi, and M. Droz, *Reaction-diffusion cellular automata model for the formation of Liesegang patterns*, Phys. Rev. Lett., 72 (1994), p. 1384.

[9] P. W. Cleary and J. J. Monaghan, *Conduction modeling using smoothed particle hydrodynamics*, J. Comput. Phys., 148 (1999), pp. 227–264.

[10] P. V. Coveney and P. W. Fowler, *Modelling biological complexity: A physical scientist's perspective*, J. R. Soc. Interface, 2 (2005), pp. 267–280.

[11] C. W. Gear, T. J. Kaper, I. G. Kevrekidis, and A. Zagaris, *Projecting to a slow manifold: singularly perturbed systems and legacy codes*, SIAM J. Appl. Dynam. Sys., 4 (2005), pp. 711–732.

[12] S. Kitsionas and A. P. Whitworth, *Smoothed Particle Hydrodynamics with particle splitting, applied to self-gravitating collapse*, Mon. Not. R. Astron. Soc., 330 (2002), pp. 129–136.

[13] P. Van Leemput, C. Vandekerckhove, W. Vanroose, and D. Roose, *Accuracy of hybrid lattice Boltzmann/finite difference schemes for reaction-diffusion systems*, SIAM J. Multiscale Model. Simul., 6 (2007), pp. 838–857.
[14] A. Malevanets and R. Kapral, *Solute molecular dynamics in a mesoscale solvent*, J. Chem. Phys., 112 (2000), pp. 7260–7269.
[15] J. J. Monaghan, *Smoothed particle hydrodynamics*, Rep. Prog. Phys., 68 (2005), pp. 1703–1759.
[16] J. J. Monaghan, H. E. Huppert, and M. G. Worster, *Solidification using smoothed particle hydrodynamics*, J. Comput. Phys., 206 (2005), pp. 684–705.
[17] S. Tang, T. Y. Hou, and W. K. Liu, *A mathematical framework of the bridging scale method*, Internat. J. Numer. Meth. Engrg., 65 (2006), pp. 1688–1713.
[18] A. M. Tartakovsky, P. Meakin, and T. Scheibe, *Simulations of reactive transport and precipitation with smoothed particle hydrodynamics*, J. Comput. Phys., 222 (2007), pp. 654–672.
[19] S. Whitaker, *The Method of Volume Averaging*, Springer-Verlag, New York, 1999.